• Basic Research •

Alterations of the vitreous pathology and anterior chamber angle structures following transscleral cyclophotocoagulation

Xiao-Wei Yu, Zhi-Jun Li, Dan-Ting Lin, Yan Gao, Jia-Xin Tian, Zhi-Gang Fan, Yan Shi

Beijing Tongren Eye Center Research Ward, Beijing Tongren Hospital, Beijing Institute of Ophthalmology, Beijing Ophthalmology & Visual Sciences Key Laboratory, Capital Medical University, Beijing 100730, China

Co-first Authors: Xiao-Wei Yu and Zhi-Jun Li

Correspondence to: Zhi-Gang Fan and Yan Shi. Beijing Tongren Hospital, 1 Dongjiaominxiang Street, Dongcheng District, Beijing 100730, China. fanzhigang@mail.ccmu.edu.cn; yansmile4433@163.com

Received: 2024-12-09 Accepted: 2025-08-20

Abstract

● **AIM:** To describe the alterations of the vitreous pathology and anterior chamber (AC) angle structures following transscleral cyclophotocoagulation (TSCP) and better understand the mechanism of post-laser intraocular pressure (IOP) reduction in angle-closure glaucoma (ACG).

● **METHODS:** Porcine eyes *ex vivo* and rabbit eyes *in vivo* were used. In porcine eyes, permeability rates of the anterior vitreous cortex (AVC) and anterior hyaloid membrane (AHM) were assessed using Schirmer's strips. Permeability rates in the circumlental space were compared with or without TSCP bursts. Fluorescein diffusion times from the vitreous to the AC were compared between eyes with and without TSCP. In rabbit eyes, changes in IOP and AC angle structures under ultrasound biomicroscopy (UBM) were evaluated at intervals of 30min, 7d, and 14d after TSCP. Vitreous pathology was examined using scanning electron microscopy (SEM) immediately and 14d after TSCP.

● **RESULTS:** In porcine eyes (n=20), the median (range) permeability rates were 10.3 (range 9.8–10.8) mm/min for the AVC and 4.3 (range 3.9–4.9) mm/min for the AHM (P=0.009). Permeability rates in the circumlental space were 4.2 (range 3.8–4.9) mm/min in areas without TSCP, 6.2 (range 5.7–6.8) mm/min in areas with non-burst TSCP, and 11.3 (range 10.9–11.8) mm/min in areas with burst TSCP (P=0.002). The median (range) fluorescein diffusion time was 5 (range 3–8)min in eyes undergoing TSCP, whereas it was 40min (range 35–68) in eyes without TSCP (P<0.001). In rabbit eyes (n=20), SEM showed immediate localized damage to the AHM, AVC, and posterior lens zonules in areas subjected to TSCP bursts, and obvious lens zonule loss with cellular infiltration and possible vitreous liquefaction by post-op day 14. Persistent widening of AC angles was noted at postoperative days 7 and 14, although a significant reduction in IOP was only observed at postoperative day 7.

● **CONCLUSION:** TSCP-induced damage on the zonules, AHM, and AVC potentially enhances fluid outflow from the vitreous, leading to a widened AC angle and vitreous liquefaction in rabbits. These observations offer insights into mechanisms of TSCP in lowering IOP and pathogenic roles of vitreous in ACG.

● **KEYWORDS:** vitreous pathology; anterior chamber angle structures; transscleral cyclophotocoagulation; angle-closure glaucoma

DOI:10.18240/ijo.2025.12.04

Citation: Yu XW, Li ZJ, Lin DT, Gao Y, Tian JX, Fan ZG, Shi Y. Alterations of the vitreous pathology and anterior chamber angle structures following transscleral cyclophotocoagulation. *Int J Ophthalmol* 2025;18(12):2246-2254

INTRODUCTION

Transscleral cyclophotocoagulation (TSCP) is a glaucoma procedure that uses laser energy to destroy the ciliary body and lower intraocular pressure (IOP). It could be widely used in both angle-closure glaucoma (ACG) and open angle glaucoma (OAG) regarding this mechanism. Previous studies suggested it was typically effective to lower IOP in patients with malignant glaucoma, acute primary angle closure (APAC), advanced primary angle-closure glaucoma (PACG), and refractory glaucoma[1-5]. In a notable case of autosomal recessive bestrophinopathy with ACG, we detected that TSCP-induced destruction of anterior vitreous and subsequent vitreous liquefaction might account for all the observed alterations following TSCP treatment, such as decreased IOP, deepened anterior chamber (AC) and angle, and rehabilitated

retinoschisis in both eyes[6]. Furthermore, in patients experiencing prolonged APAC, the immediate reduction in IOP and opening of the AC angle following low-dose TSCP may also be attributed to its impact on the anterior vitreous[5]. These findings not only provide insights into a novel mechanism of TSCP in lowering IOP but also underscore the role of the vitreous in the pathogenesis of ACG and malignant glaucoma, as suggested by previous studies. These studies have proposed that posterior forces, such as increased pressure from choroidal expansion in the presence of intact and unliquefied vitreous, contribute to angle closure, particularly in cases of malignant glaucoma and APAC[5,7-11]. Given the gaps in knowledge regarding the role of the vitreous in ACG pathophysiology and potential laser-induced vitreous changes following TSCP, we sought to study the microstructural changes of vitreous following TSCP and their effect on the vitreous pathology and AC angle structures.

MATERIALS AND METHODS

Ethical Approval All procedures were performed in accordance with ARVO Statement for the Use of Animals in Ophthalmic and Vision Research and approved by the Institutional Animal Care and Use Committee of the Capital Medical University in Beijing (approval number AEEI–2023–216).

Animals Porcine eyes were obtained from a butcher (Beijing Meat Factory) within 1d of slaughter. Pigmented, male chinchilla bastard rabbits (n=10) at the age of 12wk (body weight 2000–2500 g) were supplied from Beijing Long'an Laboratory Animal Breeding Center. Each male rabbit was raised in a single cage measuring 50 cm×60 cm×40 cm, and a nipple drinker was provided for clean water. The rabbits were fed in the morning and afternoon, every day, with commercial pellets. The rabbits were maintained under controlled conditions of approximately 27°C temperature and 40%–60% humidity on a 12-hour/12-hour light/dark cycle.

***Ex vivo* TSCP (Porcine Eyes) and *in vivo* TSCP (Rabbit Eyes)** In explanted porcine eyes, TSCP was performed by the same surgeon (Shi Y) using the OcuLight SLx 810 nm diode laser photocoagulator and the handheld fiberoptic G-probe (Iris Medical Instruments, Mountain View, CA, USA) using a power of 3.0 W and duration of 2s, which was the previously titrated power to cause an audible burst in porcine eyes[12]. This was performed in standard fashion as previously described with the probe positioned 1 mm posterior to the corneal limbus[13]. Since not every application in an eye using this power could cause an audible burst, eyes both with and without audible bursts at different parts were selected to undergo biomicroscopy and permeability tests, and untreated areas were used as controls in the same eye.

Rabbits received topical ocular anesthesia with proparacaine hydrochloride (0.5%) before TSCP. Ten TSCP applications were performed by the same surgeon (Shi Y) at a limbus distance of 0.3 mm[14], evenly distributed over the superior and inferior regions while avoiding the 2–4 o'clock and 8–10 o'clock positions. The treatment was performed using a power of 1.0 W and 2s duration, which could cause an audible burst during treatment as previously titrated. Eyes with at least 5 audible bursts were selected. Postoperatively, tobramycin-dexamethasone eye drops were prescribed 4 times daily for one week.

***Ex vivo* Permeability Rate of Anterior Hyaloid Membrane and Anterior Vitreous Cortex** The treatment area for TSCP typically focuses on the pars plicata, located at the base of the vitreous behind the ciliary processes, as previously described[15]. However, due to the difficulty of precisely separating the anterior hyaloid membrane (AHM) and the anterior vitreous cortex (AVC) at this location, we chose to evaluate the *ex vivo* permeability of AHM and AVC in the area posterior to the lens. Five intact porcine eyes were obtained and the cornea, the iris, the anterior capsule of the lens, and the nucleus were removed using microscissors and capsulorrhexis forceps. Subsequently, two-thirds of the posterior lens capsule (PLC) and one-third of the underlying AHM were removed to create an interface consisting of one-third PLC, one-third AHM, and one-third AVC (Figure 1A). After drying the surfaces across these interfaces, Schirmer's strips were centrally positioned within each region to assess permeability without contacting water extruded from the circumlental space (Figure 1B). The permeability rate was determined based on the distance of wetting in millimeters after one minute.

***Ex vivo* Biomicroscopy During TSCP (Porcine Eyes)** Porcine eyes used in the test for permeability rate of AHM and AVC were further incised sagittally. Tissue alterations at the pars plicata were observed directly under 4× magnification during TSCP with and without audible bursts.

***Ex vivo* Permeability Rate of the Circumlental Space and Fluorescein Diffusion Time from the Vitreous to the Anterior Chamber (Porcine Eyes)** Intravitreal injection of 10 μL sodium fluorescein (10%, Alcon, Tokyo, Japan) into the posterior vitreous was performed using a 27-gauge needle at 2 mm away from the optic in fifteen porcine eyes. The cornea and iris of five eyes were removed after TSCP, while the lens was intact to avoid any damage to the zonules. Then the permeability rates within the circumlental space were evaluated in untreated areas, as well as in areas treated with and without audible bursts. Permeability rate was determined as the distance of wetting in millimeters after one minute, along with recording the presence of fluid containing sodium fluorescein on Schirmer's strips.

Another 10 eyes were incubated in 37°C water to allow for the diffusion of fluorescein within the vitreous. Following 30min

of incubation, five eyes underwent TSCP while the remaining five did not, with incubation continued. The time required to identify detectable fluorescein in the AC and its dispersion pattern were recorded and compared between eyes with and without TSCP.

Ultrasound Biomicroscopy and Intraocular Pressure Alterations in AC angle structures under ultrasound biomicroscopy (UBM, model SW-3200L; Tianjin Suowei Electronic Technology Co., Ltd., Tianjin, China) and IOP measured by ICare® TONOVET (TV01; ICare Finland Oy) rebound tonometer were examined at intervals of 30min, 7 and 14d *in vivo* after TSCP, utilizing 12 eyes from 6 living rabbits. The UBM was performed in a dimly lit room in a supine position under topical anesthesia using 0.5% proparacaine. The UBM was equipped with a single element mechanical linear scanner and its frequency of the probe transducer was 50 MHz. Radial scans at the superior (with TSCP) and temporal (without TSCP) positions were performed. For each eye, at least 5 images were saved for each site and the optimal image at each site was used for measurement. Anterior chamber depth (ACD) is measured from the corneal endothelium to the anterior lenticular surface centered over the pupil; trabecular-iris angle (TIA) is measured between the scleral spur and the two endpoints of the angle opening distance; trabecular ciliary process angle (TCPA) is measured with its apex at the scleral spur, one arm along the posterior corneal surface, and another arm along the most anterior surface of the ciliary body; trabecular-ciliary processes distance 750 (TCPD750) is defined as the length of a line extending from the trabecular meshwork at 750 μm from the scleral spur perpendicularly through the iris to the surface of the ciliary process; angle opening distance 750 (AOD750) is the distance between the inner corneal surface and the anterior iris surface measured on a line perpendicular to the plane of the trabecular meshwork at 750 μm from the scleral spur[16].

Scanning Electron Microscopy Two rabbits were sacrificed immediately following TSCP and the other two were sacrificed 14d after TSCP with inhalation of excessive CO_2. Eyes were enucleated and then fixed in a solution of 2.5% glutaraldehyde (0.1 mol/L phosphate buffer solution) at room temperature for 2h and 4°C overnight. After fixation, one eye from each rabbit was washed in phosphate buffer solution and bisected along the equator, separating the eye into anterior and posterior portions used to evaluate the AHM and anterior vitreous, respectively. The other eye of each rabbit was incised sagittally from the 12 to 6 o'clock direction while maintaining the integrity of the natural lens and vitreous anatomy. Specimens were rinsed in 1% osmium tetroxide solution at room temperature for 1h then dehydrated in a graded ethanol series and dried in a critical point dryer (Leica EM CPD300). The specimens were then mounted on aluminum stubs using colloidal silver liquid and sputter coated with a thin film of gold/palladium and were observed using field emission scanning electron microscopy (SEM; Thermo Fisher FEI Quanta FEG 450). TSCP areas without audible bursts and untreated areas of the eyes were used as controls for TSCP areas with audible bursts.

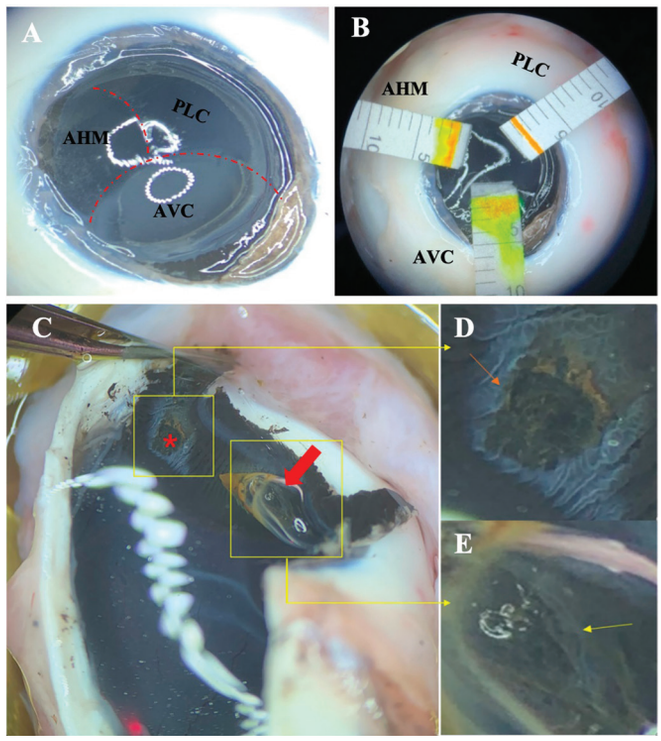

Figure 1 Permeability rate of AHM and AVC and biomicroscopic changes during TSCP in porcine eyes A: Image demonstrating the three tissue interfaces. B: Permeability rate of three interfaces measured by Schirmer's strip for 1min. The permeability rate of the posterior capsule was 0, meaning liquid could not penetrate the PLC. C: Areas treated with TSCP with an audible burst (red star) and without an audible burst (red arrow). At the site where a bubble ruptured caused an audible sound (red star). While at the site where a bubble did not rupture, pigment aggregated within the bubble. D: Magnified view of 1C showing the adjacent non-pigmented ciliary epithelium became edematous (orange arrow). E: Magnified view of 1C showing the bubble that formed between the ciliary epithelium and AHM during TSCP without an audible burst (red arrow in 1C), the underlying non-pigmented ciliary epithelium was also damaged but did not show obvious edema (yellow arrow). PLC: Posterior lens capsule; AHM: Anterior hyaloid membrane; AVC: Anterior vitreous cortex; TSCP: Transscleral cyclophotocoagulation.

Statistical Analysis All statistical analyses were performed using SPSS (V.24.0; SPSS, Chicago, IL, USA). The Mann-Whitney *U* and Kruskal-Wallis *H* tests were used to compare groups. Wilcoxon Signed-Rank Test was used to compare IOP and UBM parameters. $P<0.05$ were considered statistically significant.

Table 1 Anterior chamber angle parameters of rabbit eyes following TSCP

Parameters	Before TSCP	30min after TSCP		7d after TSCP		14d after TSCP	
	Median (range)	Median (range)	*P*1	Median (range)	*P*2	Median (range)	*P*3
ACD (mm)	2.44(2.25, 2.62)	2.52 (2.44, 2.60)	0.488	2.39 (2.26, 2.54)	0.544	2.42 (2.25, 2.52)	0.538
TIA-S (degree)	17.99 (15.19, 20.88)	22.00 (17.76, 27.21)	0.094	27.24 (25.46, 28.78)	0.001[a]	29.70 (20.52, 31.22)	0.006[a]
TIA-T (degree)	18.50 (12.67, 20.19)	23.60 (17.87, 27.94)	0.065	28.38 (19.96, 31.03)	0.005[a]	22.37 (19.14, 28.68)	0.012[a]
TCPA-S (degree)	45.48 (39.36, 49.05)	46.31 (42.49, 51.94)	0.248	52.43 (46.03, 61.29)	0.011[a]	58.23 (49.08, 62.67)	0.007[a]
TCPA-T (degree)	45.97 (39.31, 50.07)	47.78 (44.13, 53.79)	0.248	51.65 (43.78, 58.78)	0.057	54.94 (44.53, 64.56)	0.049[a]
TCPD-S (mm)	0.55 (0.41, 0.58)	0.59 (0.39, 0.85)	0.285	0.76 (0.60, 0.86)	0.003[a]	0.64 (0.59, 0.83)	0.001[a]
TCPD-T (mm)	0.51 (0.36, 0.56)	0.60 (0.41, 0.82)	0.236	0.76 (0.66, 0.78)	0.001[a]	0.73 (0.59, 0.85)	0.002[a]
AOD750-S (mm)	0.32 (0.24, 0.35)	0.33 (0.25, 0.40)	0.488	0.37 (0.30, 0.44)	0.088	0.41 (0.29, 0.45)	0.065
AOD750-T (mm)	0.33 (0.25, 0.35)	0.34 (0.27, 0.39)	0.643	0.39 (0.29, 0.43)	0.140	0.33 (0.27, 0.43)	0.339
IOP (mm Hg)	16.50 (14.00, 18.75)	30.95 (27.50, 33.47)	<0.001[b]	11.50 (10.00, 13.00)	<0.001[b]	14.17 (14.00, 14.17)	0.080

TSCP: Transscleral cyclophotocoagulation; ACD: Anterior chamber depth; TIA: Trabecular-iris angle; TCPA: Trabecular ciliary process angle; TCPD: Trabecular-ciliary processes distance; AOD750: Angle opening distance 750; S: Superior; T: Temporal; IOP: Intraocular pressure. *P* values were compared to the eyes before TSCP using Wilcoxon signed-rank test. [a]*P*<0.05; [b]*P*<0.001.

RESULTS

***Ex vivo* Permeability Rates of AHM and AVC in Porcine Eyes Without TSCP** In porcine eyes that were not subjected to TSCP, the highest permeability rate was observed in the AVC at 10.3 mm/min (range: 9.8–10.8), followed by the AHM at 4.3 mm/min (range: 3.9–4.9, *P*=0.009). The permeability rate of the PLC was recorded as 0, indicating no penetration of liquid through the posterior capsule (Figure 1B).

***Ex vivo* Biomicroscopy in Porcine Eyes During TSCP** Under biomicroscopy, the localized destruction of ciliary pigmented and non-pigmented epithelium, and underlying pigmented tissues were observed at the treatment site both with and without burst during TSCP. Moreover, we observed a bubble formed between the ciliary epithelium and AHM, with the audible burst corresponding to its rupture (Figure 1C). Subjectively, the volume of the ruptured bubble correlated with the intensity of the sound, while bubbles that formed during TSCP but did not rupture did not produce any sound or audible burst, indicating that the noise originated from the rupture of the AHM and AVC. Edema of the non-pigmented ciliary epithelium was observed where the bubble ruptured (Figure 1C and 1D), while pigment aggregated within the bubble with no obvious non-pigmented ciliary epithelium edema at the site where the bubble did not rupture (Figure 1E).

***Ex vivo* Permeability Rate and Fluorescein Dispersion Rate in Porcine Eyes Following TSCP** Following TSCP, the median permeability rates at the circumlental space in five porcine eyes were as follows: 4.2 mm/min (range: 3.8–4.9) in the untreated portion, 6.2 mm/min (range: 5.7–6.8) in the region subjected to TSCP without audible bursts, and 11.3 mm/min (range: 10.9–11.8) in the area receiving TSCP with audible bursts (*P*=0.002). Additionally, only the Schirmer's strips placed in the area with TSCP bursts exhibited sodium fluorescein (Figure 2A–2C).

The median time required for fluorescein diffusion into the AC was 5min (range: 3–8min) in eyes undergoing TSCP, with initial detection and notably high concentration observed at the pupil margin in the direction of TSCP with audible bursts. In contrast, the median time for fluorescein diffusion into the AC was 40min (range: 35–68min, *P*<0.001) in eyes without TSCP, with a uniform distribution and low concentration observed around the pupil margin (Figure 2E and 2F).

Widening of the Anterior Chamber Angle Structures and IOP Fluctuations After TSCP The alterations in AC angle parameters and IOP subsequent to TSCP in rabbit eyes were presented in Table 1. Thirty minutes after TSCP, no significant difference in AC angle parameters was detected, while the median IOP was increased from 16.50 (range: 13–21) mm Hg to 31.95 (range: 24–51, *P*<0.001) mm Hg. On the 7th day post-TSCP, significant increases of TIA, TCPD750 of both superior and temporal quadrants, TCPA of the superior quadrant (TCPA-S), and reduction of IOP were observed compared to pre-TSCP measurements (all *P*<0.05). On the 14th day post-TSCP, these UBM parameters were still significantly increased (all *P*<0.05), and the IOP recovered to the same level as that of the pre-TSCP values (*P*=0.08). Additionally, when comparing all parameters between the superior (S) and temporal (T) regions at any interval, no statistically significant differences were found (*P*>0.05).

Alterations in the Vitreous Observed Under SEM Following TSCP In comparison to rabbit eyes assessed immediately after TSCP, those evaluated 14d post-TSCP exhibited a more liquefied vitreous and less gelatinous consistency during eyeball bisection, indicating vitreous liquefaction following TSCP. Immediately after TSCP, SEM revealed the destruction of AHM and AVC at the site of TSCP with audible bursts in the area of the pars plicata (Figure 3A and 3B). Additionally, adjacent posterior lens zonules displayed damage with cellular

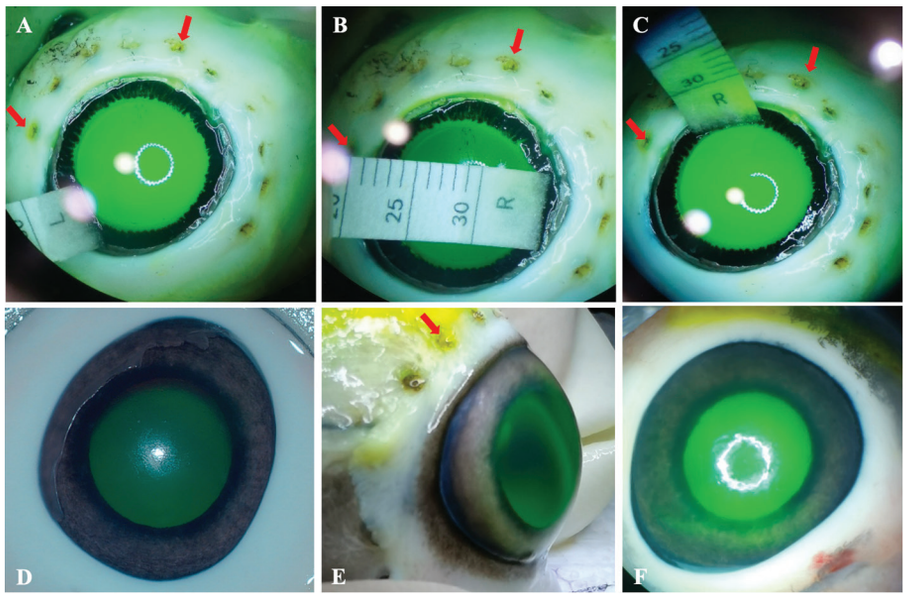

Figure 2 Permeability rate of the circumlental space and fluorescein diffusion time from the vitreous to the AC (porcine eyes) A: The permeability rate within the circumlental space in the untreated area was evaluated by Schirmer's strip for 1min, no sodium fluorescein was detected on the strip. The superficial dark spots on the sclera represent the locations of TSCP treatment. The red arrows indicate points with an audible burst. B: The permeability rate within the circumlental space in the area treated without audible bursts was evaluated by Schirmer's strips for 1min. No apparent presence of sodium fluorescein was detected on the strip. C: The permeability rate within the circumlental space in area treated with audible bursts was evaluated by Schirmer's strip for 1min. Sodium fluorescein was clearly evident on the Schirmer's strip. D: Following 30min of incubation in 37°C water, no sodium fluorescein was detected in the AC. E: Following 30min of incubation in 37°C water and subsequent TSCP, the median time required for fluorescein diffusion into the AC was 5min (range: 3–8min) in porcine eyes, with initial detection and notably high concentration observed at the pupil margin in the direction of TSCP with audible bursts. F: Following 30min of incubation in 37°C water, the median time for fluorescein diffusion into the AC was 40min (range: 35–68min) in eyes without TSCP, with a uniform distribution and low concentration observed around the pupil margin. AC: Anterior chamber; TSCP: Transscleral cyclophotocoagulation.

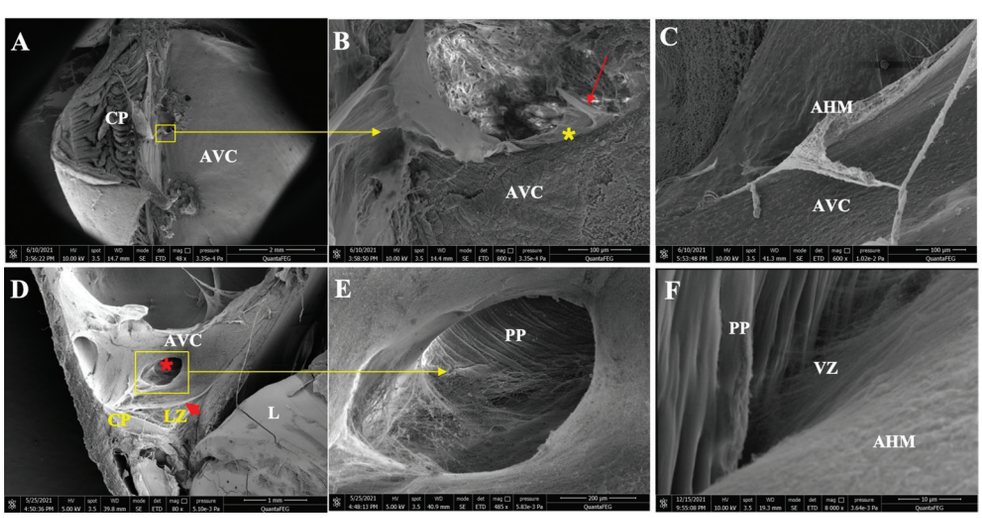

Figure 3 Scanning electron micrograph of AHM and AVC following TSCP with audible burst in rabbit eyes A: Immediately after TSCP, there was localized architectural disorganization of the ciliary body with adjacent destruction of the AHM and AVC at the site of TSCP with burst. The CP were intact. B: Magnified view of 3A showing ruptured AHM (red arrow) and defect in the AVC (yellow star). C: Thinner AVC after 14d compared with that in 3B. D: A cavitation (red star) with a smooth edge was identified immediately after TSCP between ciliary epithelium and AHM in the region subjected to TSCP without audible bursts. Red arrowhead: AHM. E: Magnified view of 3D showing the intact surface of pars plana under the cavity, which suggested the detachment of AHM at the vitreous base, potentially indicating the dispersion path of bubbles during TSCP. F: Immediately after TSCP, the AHM was connected to PP by VZ at the area without TSCP, which could only become visible by careful elevation of the posterior AHM. AHM: Anterior hyaloid membrane; AVC: Anterior vitreous cortex; TSCP: Transscleral cyclophotocoagulation; CP: Ciliary process; LZ: Lens zonule; L: Lens; PP: Pars plana; VZ: Vitreous zonule.

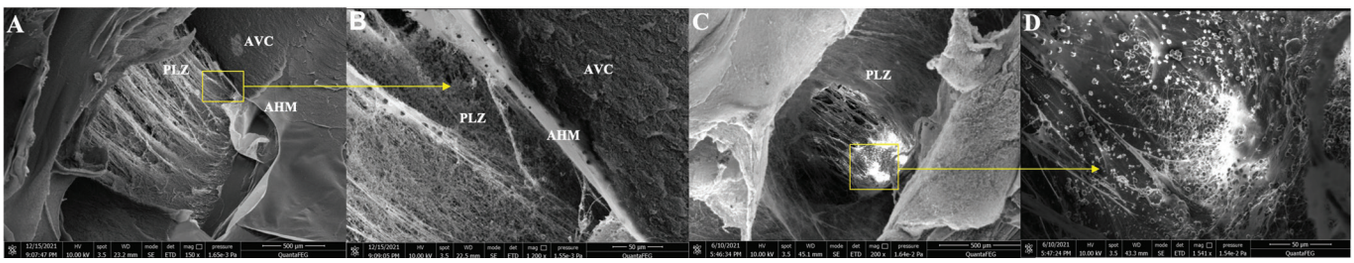

Figure 4 Scanning electron micrograph of posterior lens zonule damage immediately following and 14d after TSCP with audible burst in rabbit eyes A: Immediately following TSCP, AHM, AVC, and PLZ at the site of TSCP with burst were damaged; B: Magnified view of 4A demonstrating PLZ damage with cellular infiltration; C: Fourteen days following TSCP, more lens zonule loss was detected at the site of treatment; D: Magnified view of 4C demonstrating significant cellular infiltration in the lens zonule. AHM: Anterior hyaloid membrane; AVC: Anterior vitreous cortex; TSCP: Transscleral cyclophotocoagulation; PLZ: Posterior lens zonules.

infiltration (Figure 4A and 4B). In regions subjected to TSCP without audible bursts, AHM detachment was observed, potentially indicating the dispersion path of bubbles formed between AHM and the ciliary epithelium (Figure 3D and 3E). Conversely, in untreated areas, all structures appeared normal, with the AHM remaining attached to the pars plana, and the vitreous zonule between them remained intact (Figure 3F). The ciliary processes were intact in any region.

Evaluation 14d post-TSCP revealed localized loss of lens zonules with persistent cellular infiltration in regions treated with TSCP with audible bursts (Figure 4C and 4D). The AVC near the burst site appeared thinner compared to its state immediately after TSCP (Figure 3B and 3C). This observation suggested that vitreous liquefaction may have occurred, rendering the AVC more susceptible to dehydration compared to eyes evaluated immediately after TSCP using the same dehydration method (Figure 4A, 4C).

DISCUSSION

Here, we provide both *ex vivo* and *in vivo* evidence of vitreous changes after TSCP, including localized damage of the AHM, AVC, and lens zonule, detached vitreous base, alongside vitreous liquefaction. These findings likely contribute to increased permeability rates at the circumlental space, facilitating fluid diffusion from the vitreous into the AC. Moreover, they may explain the widening of the AC angle in rabbit eyes, which are predisposed to narrow angles due to spherical lenses, anterior rotation of ciliary processes, and subsequent iris bombe[17]. This study is the first to delineate the influence of TSCP on lowering IOP in ACG by elucidating its impact on the vitreous and subsequent alterations in AC angle structures.

The primary mechanism of IOP reduction following TSCP is believed to involve decreased aqueous humor secretion due to coagulation necrosis of the ciliary epithelium[12]. Additional mechanisms such as increased uveoscleral outflow and microinfarction of the ciliary body have been proposed[14-15]. However, despite the initial IOP decrease observed 7d after TSCP in rabbit eyes, levels returned to baseline by postoperative day 14. This could be attributed to the limited application of only 10 shots and incomplete treatment of the ciliary processes, which may not sufficiently reduce aqueous humor secretion, as observed in clinical cases undergoing TSCP[15]. Pigmented particle dispersion into the trabecular meshwork and transient over-secretion of aqueous humor post-TSCP may explain immediate IOP elevation, which is not uncommon in clinical practice[18]. Conversely, periodic increases in uveoscleral outflow could explain temporary IOP reductions followed by recovery[5]. These findings collectively enhance our understanding of the uncertain effect of TSCP on lowering IOP.

On the contrary, the widening of the AC angle observed in rabbit eyes after TSCP appears to align more closely with the sustained effectiveness of low-dosage TSCP in reducing IOP in conditions like malignant glaucoma, APAC[1,5], advanced PACG[2], and refractory glaucoma[3-4], where significant widening of AC structures are also noted, contrasting with less pronounced IOP responses seen in neovascular, traumatic, and uveitic glaucoma cases[19-20]. Our findings challenge the conventional explanation attributing angle widening to the contraction of ciliary processes and subsequent posterior displacement of the peripheral iris and a reduction in AC angle crowding[19], as we did not observe such contraction in rabbit eyes. Instead, we observed localized destruction of the pars plicata and intact ciliary processes, consistent with human eye biopsy findings post-TSCP[5]. Similar in clinical practice, the anterior rotation of ciliary processes, commonly seen in ACG and malignant glaucoma, may pose challenges to the targeting of ciliary processes in TSCP treatment. Moreover, if the contraction of ciliary processes was the primary factor, its effect on angle architecture would be limited to the treatment site, yet our rabbit eyes showed similar angle widening at both treated and untreated sites, as observed using UBM.

Previous literature has suggested that the misdirection of aqueous humor into or behind the vitreous body, along

with poor vitreous conductivity in the context of choroidal expansion, plays a pathogenic role in ACG, particularly in cases of malignant glaucoma[9]. Irido-zonule-hyaloid-vitrectomy (IZHV), a procedure that establishes communication between the anterior and posterior segments by creating an opening in the ciliary body-zonules-crystalline lens-hyaloid-anterior vitreous complex (CZLHV), has become a standard approach for preventing and managing malignant glaucoma in refractory ACG cases[10,21-24]. Our findings regarding the modifying effect of TSCP on CZLHV are consistent with the outcomes observed with IZHV, demonstrating their efficacy in managing ACG and malignant glaucoma.

In our study, we found that the AHM serves as a permeable barrier, regulating the rate of water outflow from the vitreous. Burst TSCP ruptured the AHM, and damaged the AVC, and adjacent posterior lens zonules, as confirmed by SEM, promoting fluid outflow through the circumlental space. Even non-burst TSCP points could also aid fluid outflow by increasing the permeability surface due to AHM detachment, which is caused by either bubble formation or thermomechanical damage to the vitreous zonule at the vitreous base. This explains slower Schirmer's strip wetting at non-bursting TSCP sites compared to bursting ones but faster than non-TSCP points. Additionally, fluorescein diffusion into the AC was accelerated after TSCP, particularly at bursting TSCP sites, supporting the efficacy of TSCP in conditions like APAC and malignant glaucoma, where trapped aqueous humor is evident within the vitreous[5]. These effects, akin to those of IZHV, could lead to AC deepening and angle widening[25]. Although these effects should be immediately apparent, ciliary processes edema and increased volume in the vitreous cavity due to air bubble formation may delay observable changes, as observed in rabbit eyes 30min after TSCP and our clinical practice[5].

Despite our rabbit model not perfectly mirroring conditions like ACG or malignant glaucoma, we did observe angle widening and reduced anterior rotation of ciliary processes post-TSCP over 1 to 2wk. However, the presence of the crystalline lens might limit significant AC deepening. We hypothesize that in rabbit eyes, the spherical lens shape and zonular tension mainly determine its positioning, unlike in APAC or malignant glaucoma where fluid entrapment in the vitreous was the main force pushing lens forward, particularly when primary or secondary zonulopathy frequently existed in these cases[26-27]. Our findings also suggest that the peripheral anterior vitreous may directly influence AC angle configuration *via* its effect on ciliary processes and peripheral iris, rather than lens position, in rabbit eyes. The anterior rotation of ciliary processes could indicate vitreous pressure on them, emphasizing the need to modify the CZLHV complex to prevent ACG progression and malignant glaucoma post-surgery, whether through TSCP or IZHV, in clinical settings.

Moreover, our results highlight the impact of TSCP on vitreous liquefaction. Although we couldn't quantify the degree of liquefaction directly, we observed a higher water proportion and reduced gel content in the vitreous during eyeball bisection, along with a thinner AVC under SEM, 14d post-TSCP compared to immediately after. The vitreous contains water, collagen, hyaluronic acid, and electrolytes, with higher collagen content in the anterior vitreous and vitreous base[28]. This collagen provides structural support and determines gel stiffness, enhancing internal strength[29]. Hyaluronic acid contributes to increased vitreous modulus by swelling and applying tension to the collagen network[30]. Thermomechanical damage from TSCP to the collagen network at the vitreous base may release hyaluronic acid, reducing vitreous modulus[30]. Additionally, our study observed immune cell infiltration of lens zonules and zonule loss after TSCP. Inflammation-related matrix metalloproteinases may alter collagen and hyaluronic acid structure in the zonules and vitreous[31-32]. In ACG and malignant glaucoma, these alterations could further lead to decreased vitreous conductivity during choroidal expansion and reduced anterior rotation of the ciliary processes, thus widening AC angle, as observed in our previous studies[5] and the rabbit eyes of this study. Furthermore, these findings raise concerns about choroidal effusion or exudative retinal detachment following TSCP, as the supportive role of the vitreous is compromised. Therefore, caution is warranted when considering extensive TSCP in eyes with significant vitreous liquefaction, such as those with high myopia or predisposition to uveal effusion, like in cases of nanophthalmos.

There are several limitations to this study. First, although porcine and rabbit vitreous structures resemble that of humans, the translatability of these results to humans is unclear. Second, although we intended to interpret our findings in ACG due to the role of vitreous in causing angle closure, our study couldn't justify that for rabbit is still not a real ACG animal model. In fact, laser-induced vitreous changes following TSCP may be similar in both angle closure or open angle eyes. Further research is still needed to determine how these results translate to humans with ACG and other forms of glaucoma. Third, factors such as laser power, duration, and the presence of an audible burst may vary in real world conditions and not correspond directly to the histologic findings presented here.

In summary, our study presents the first evidence of *ex vivo* and *in vivo* damage induced by TSCP to the zonules, AHM, and AVC. This damage correlates with increased fluid outflow from the vitreous through the circumlental space in porcine eyes *ex vivo*, widening of AC angle structures, alleviation

of the anterior rotation of the ciliary processes, and vitreous liquefaction, irrespective of postoperative IOP fluctuations in rabbit eyes *in vivo*. These findings potentially explain the mechanism behind IOP regulation in ACG *via* TSCP, while also highlighting the pathogenic role of vitreous in ACG, especially in APAC and malignant glaucoma cases.

ACKNOWLEDGEMENTS

The authors thank the National Center for Protein Sciences at Peking University in Beijing, China, for invaluable help in preparing the specimens for SEM investigations and Yi-Qun Liu, Peng-Yuan Dong, Yi-Feng Jiang, and Hong-Mei Zhang for technical assistance.

Authors' Contributions: Yu XW, Fan ZG, and Shi Y designed the study; Yu XW, Li ZJ, Lin DT, Gao Y, and Tian JX performed the experiments and analyzed the data; Yu XW, Li ZJ, Lin DT, and Shi Y wrote the manuscript; Fan ZG and Shi Y obtained fundings. All authors read and approved the final manuscript.

Foundations: Supported by National Natural Science Foundation of China (No.82201171; No.82171050; No.82471072).

Conflicts of Interest: Yu XW, None; **Li ZJ,** None; **Lin DT,** None; **Gao Y,** None; **Tian JX,** None; **Fan ZG,** None; **Shi Y,** None.

REFERENCES

1 Liu W, Qin LN, Xu CJ, *et al*. Transscleral cyclophotocoagulation followed by cataract surgery: a novel protocol to treat refractory acute primary angle closure. *BMC Ophthalmol* 2020;20(1):209.

2 Fili S, Kontopoulou K, Vastardis I, *et al*. Transscleral cyclophotocoagulation with MicroPulse® laser versus Ahmed valve implantation in patients with advanced primary open-angle glaucoma. *Int Ophthalmol* 2021;41(4):1271-1282.

3 Al Owaifeer AM, Almutairi AT, Schargel K. The outcomes of transscleral cyclophotocoagulation in pediatric glaucoma secondary to Sturge-Weber syndrome. *J Am Assoc Pediatr Ophthalmol Strabismus* 2022;26(2):78.e1-78.e5.

4 Banifatemi M, Nilforushan N, Sedaghat A, *et al*. Trans-scleral cyclophotocoagulation in refractory pigment dispersion-like glaucoma secondary to ciliary body melanoma. *J Curr Ophthalmol* 2022;34(1):118-120.

5 Shi Y, Oatts J, Tian J, *et al*. Low-dose transscleral cyclophotocoagulation with subsequent phacoemulsification in the treatment of prolonged acute primary angle closure. *Br J Ophthalmol* 2023;107(2):221-226.

6 Shi Y, Tian JX, Han Y, *et al*. Pathogenic role of the vitreous in angle-closure glaucoma with autosomal recessive bestrophinopathy: a case report. *BMC Ophthalmol* 2020;20(1):271.

7 Robert R, Lowe RF. Angle-closure glaucoma: mechanisms and epidemiology. In: Ritch R, Shields MB, Krupin T, eds. *The Glaucomas*. St Louis: CV Mosby Co; 1996.

8 Grant WM. Experimental aqueous perfusion in enucleated human eyes. *Arch Ophthalmol* 1963;69:783-801.

9 Quigley HA, Friedman DS, Congdon NG. Possible mechanisms of primary angle-closure and malignant glaucoma. *J Glaucoma* 2003;12(2):167-180.

10 Yu XW, Zhao ZN, Zhang DD, *et al*. Anterior vitrectomy, phacoemulsification cataract extraction and irido-zonulo-hyaloid-vitrectomy in protracted acute angle closure crisis. *Int Ophthalmol* 2021;41(9):3087-3097.

11 Krix-Jachym K, Żarnowski T, Rękas M. Risk factors of malignant glaucoma occurrence after glaucoma surgery. *J Ophthalmol* 2017;2017(1):9616738.

12 Dastiridou AI, Katsanos A, Denis P, *et al*. Cyclodestructive procedures in glaucoma: a review of current and emerging options. *Adv Ther* 2018;35(12):2103-2127.

13 Ahn SM, Choi M, Kim SW, *et al*. Changes after a month following micropulse cyclophotocoagulation in normal porcine eyes. *Transl Vis Sci Technol* 2021;10(13):11.

14 Schlote T, Beck J, Rohrbach JM, *et al*. Alteration of the vascular supply in the rabbit ciliary body by transscleral diode laser cyclophotocoagulation. *Graefes Arch Clin Exp Ophthalmol* 2001;239(1):53-58.

15 McKelvie PA, Walland MJ. Pathology of cyclodiode laser: a series of nine enucleated eyes. *Br J Ophthalmol* 2002;86(4):381-386.

16 Guo CC, Zhao ZN, Zhang DD, *et al*. Anterior segment features in nanophthalmos with secondary chronic angle closure glaucoma: an ultrasound biomicroscopy study. *Invest Ophthalmol Vis Sci* 2019;60(6):2248-2256.

17 Bouhenni RA, Dunmire J, Sewell A, *et al*. Animal models of glaucoma. *J Biomed Biotechnol* 2012;2012:692609.

18 Razeghinejad MR, Hamid A, Nowroozzadeh MH. Immediate IOP elevation after transscleral cyclophotocoagulation. *Eye* (*Lond*) 2017;31(8):1249-1250.

19 Schlote T, Derse M, Rassmann K, *et al*. Efficacy and safety of contact transscleral diode laser cyclophotocoagulation for advanced glaucoma. *J Glaucoma* 2001;10(4):294-301.

20 Souissi S, Le Mer Y, Metge F, *et al*. An update on continuous-wave cyclophotocoagulation (CW-CPC) and micropulse transscleral laser treatment (MP-TLT) for adult and paediatric refractory glaucoma. *Acta Ophthalmol* 2021;99(5):e621-e653.

21 Tang YZ, Gao Y, Yu XW, *et al*. Novel diagnostic indicators for acute angle closure secondary to lens subluxation based on anterior segment and lens parameters. *Heliyon* 2024;10(3):e25164.

22 Raj S, Thattaruthody F, Joshi G, *et al*. Treatment outcomes and efficacy of pars Plana vitrectomy-hyaloidotomy-zonulectomy-iridotomy in malignant glaucoma. *Eur J Ophthalmol* 2021;31(1):234-239.

23 Jin SW, Caprioli J. Long-term treatment outcomes for malignant glaucoma. *Ophthalmol Glaucoma* 2024;7(3):282-289.

24 Schmidt DC, Kessel L, Pedersen KB, *et al*. Pars Plana vitrectomy combined with hyaloido-zonula-iridectomy in treatment of patients with chronic aqueous misdirection: a systematic literature review and case series. *Acta Ophthalmol* 2021;99(3):251-259.

25 Nonaka A, Kondo T, Kikuchi M, *et al*. Angle widening and alteration of ciliary process configuration after cataract surgery for primary angle closure. *Ophthalmology* 2006;113(3):437-441.

26 Nagae K, Sawamura H, Aihara M. Investigation of intraocular pressure of the anterior chamber and vitreous cavity of porcine eyes *via* a novel method. *Sci Rep* 2020;10(1):20552.

27 Silver DM, Quigley HA. Aqueous flow through the iris-lens channel: estimates of differential pressure between the anterior and posterior chambers. *J Glaucoma* 2004;13(2):100-107.

28 Ramsay E, Lajunen T, Bhattacharya M, *et al*. Selective drug delivery to the retinal cells: biological barriers and avenues. *J Control Release* 2023;361:1-19.

29 Levin M, Cohen N. The effects of aging on the mechanical properties of the vitreous. *J Biomech* 2021;119:110310.

30 Nickerson CS, Park J, Kornfield JA, *et al*. Rheological properties of the vitreous and the role of hyaluronic acid. *J Biomech* 2008;41(9):1840-1846.

31 Ohta Y, Hayashi M, Kanemaru T, *et al*. Dual modulation of airway smooth muscle contraction by Th2 cytokines *via* matrix metalloproteinase-1 production. *J Immunol* 2008;180(6):4191-4199.

32 Ren Y, Zhang H, Qin WJ, *et al*. A collagen mimetic peptide-modified hyaluronic acid hydrogel system with enzymatically mediated degradation for mesenchymal stem cell differentiation. *Mater Sci Eng C Mater Biol Appl* 2020;108:110276.